A constrained extended Kalman filter for the optimal estimate of kinematics and kinetics of a sagittal symmetric exercise

Vincent V. Bonnet, Raphaël Dumas, Aurelio Cappozzo, Vladimir Joukov, Gautier Daune, Dana Kulić, Philippe Fraisse, Sébastien Andary, Gentiane Venture

www.elsevier.com/locate/jbiomech

A constrained extended Kalman filter for the optimal estimate of kinematics and kinetics of a sagittal symmetric exercise

V. Bonnet, R. Dumas, A. Cappozzo, V. Joukov, G. Daune, D. Kulić, P. Fraisse, S. Andary, G. Venture

PII: S0021-9290(16)31320-3
DOI: http://dx.doi.org/10.1016/j.jbiomech.2016.12.027
Reference: BM8060

To appear in: *Journal of Biomechanics*

Received date: 18 April 2016
Revised date: 14 December 2016
Accepted date: 19 December 2016

Cite this article as: V. Bonnet, R. Dumas, A. Cappozzo, V. Joukov, G. Daune, D. Kulić, P. Fraisse, S. Andary and G. Venture, A constrained extended Kalman filter for the optimal estimate of kinematics and kinetics of a sagittal symmetri exercise, *Journal of Biomechanics* http://dx.doi.org/10.1016/j.jbiomech.2016.12.027

A constrained extended Kalman filter for the optimal estimate of kinematics and kinetics of a sagittal symmetric exercise

V. Bonnet[1*], R. Dumas[2,3], A. Cappozzo[3,4], V. Joukov[5], G. Daune[6], D. Kulić[5], P. Fraisse[7], S. Andary[8], G. Venture[6]

[1]University of Paris-Est Créteil, Laboratory of Image, Signal and Intelligent Systems, LISSI, France

[2]Univ Lyon, Université Claude Bernard Lyon 1, IFSTTAR, UMR_T9406, LBMC, F69622, Lyon, France

[3]Interuniversity Centre of Bioengineering of the Human Neuromusculoskeletal System, Università degli Studi di Roma "Foro Italico", Italia

[4]Department of Movement, Human, and Health Sciences, Università degli Studi di Roma "Foro Italico", Italia

[5]Department of Electrical and Computer Engineering, University of Waterloo, Canada

[6]Department of Mechanical Systems Engineering, Tokyo University of Agriculture and Technology, Japan

[7]LIRMM UMR 5506 CNRS, Montpellier University, France.

[8]NaturalPad, Montpellier, France

vincent.bonnet@u-pec.fr

pietro.cerveri@biomed.polimi.it

floren.colloud@univ-poitiers.fr

friedl.degroote@kuleuven.be

[*]Corresponding author. Vincent Bonnet. Université Paris-Est-Créteil, Laboratoire Images, Signaux et Systèmes Intelligents (LISSI) - EA 3956, Domaine Chérioux, 122 rue Paul Armangot, 94400 Vitry sur Seine, France.

ABSTRACT

This paper presents a method for real-time estimation of the kinematics and kinetics of a human

body performing a sagittal symmetric motor task, which would minimize the impact of the stereophotogrammetric soft tissue artefacts (STA). The method is based on a bi-dimensional mechanical model of the locomotor apparatus the state variables of which (joint angles, velocities and accelerations, and the segments lengths and inertial parameters) are estimated by a constrained extended Kalman filter (CEKF) that fuses input information made of both stereophotogrammetric and dynamometric measurement data. Filter gains are made to saturate in order to obtain plausible state variables and the measurement covariance matrix of the filter accounts for the expected STA maximal amplitudes. We hypothesised that the ensemble of constraints and input redundant information would allow the method to attenuate the STA propagation to the end results. The method was evaluated in ten human subjects performing a squat exercise. The CEKF estimated and measured skin marker trajectories exhibited a RMS difference lower than 4 mm, thus in the range of STAs. The RMS differences between the measured ground reaction force and moment and those estimated using the proposed method (9 N and 10 Nm) were much lower than obtained using a classical inverse dynamics approach (22 N and 30 Nm). From the latter results it may be inferred that the presented method allows for a significant improvement of the accuracy with which kinematic variables and relevant time derivatives, model parameters and, therefore, intersegmental moments are estimated.

Keywords

Extended Kalman Filter, Inverse kinematics, Inverse dynamics, Inertial parameters identification

1 Introduction

Stereophotogrammetric systems, which consist of multiple cameras able to track the location of markers placed on the body segments, allow the estimate of the instantaneous pose of bones and joint kinematics. Given a mechanical model of the locomotor apparatus, this kinematic information and measured external forces allow the estimate of joint kinetics through a bottom-up recursive Newton-Euler method. Alternatively, when the motion analysed is monopodalic or symmetric in the sagittal plane, a top-down recursive Newton-Euler method, which relies on

kinematic data only, may be used.

Whatever the method used, the estimate of joint kinetics suffers from the following major types of inaccuracies. One is related to the definition of the locomotor apparatus mechanical model. In particular, the geometric parameters, i.e. location of the joint centres and segment lengths, and body segment inertial parameters (BSIP: masses, positions of the centres of mass, and moments of inertia) are normally estimated using readily measurable anthropometric quantities and regression equations or geometric approximation, leading to limited accuracy (Robert et al., 2007). The marker trajectories provided by stereophotogrammetric systems may be very accurate (Fohanno et al., 2014), however, the movement of the markers attached to the skin relative to the underlying bones, known as soft-tissue-artefact (STA), heavily degrades the estimation of bone pose (Stagni et al., 2000; Riemer et al., 2008; Lamberto et al., 2016). Lastly, the algorithms used to estimate first and second time derivatives of noisy position data also introduce errors.

Cahouet et al. (2002) and Kuo (1998) have proposed a least-squares approach that adjusts the accelerations so that the error with which the Ground Reaction Forces and Moments (GRFM) are estimated using inverse dynamics is minimized. However, this approach may produce unrealistic accelerations since the algorithm, besides compensating for the differentiation error, concurrently compensates for the ensemble of the other above-mentioned error sources.

Multi-body optimization is widely used to estimate instantaneous bone pose while reducing the impact of STA (Lu and O'Connor, 1999). This method controls joint movement but does not optimize time derivatives nor model parameters. The Extended Kalman Filter (EKF) has been proposed as an alternative for computing joint angles, velocities, and accelerations on-line (Cerveri et al., 2005; Ayusawa et al., 2013). Contrary to multi-body optimization, constraining variables in an EKF, for example ensuring that joint angles are within a plausible range, is not trivial (Simon, 2010). Regarding STA compensation, Cerveri et al. (2005) showed, although using simulated data only, that introducing the marker positions relative to the bone-embedded frames in the EKF's state vector and an appropriate adjustment of the EKF parameters can reduce the STA impact on bone pose estimation by up to 50%.

In this study, we propose a method to estimate the joint angles, velocities and accelerations, the segments lengths, local marker positions, and inertial parameters (state variables) by a

constrained extended Kalman filter (CEKF) that fuses input information from both stereophotogrammetric skin-marker trajectories and dynamometric measurement data. The method, based on a bi-dimensional mechanical model of the locomotor apparatus, produces state variable values that are jointly constrained to be consistent with the kinetics of the movement as summarized by the ground reactions. The specific contributions of this paper are:

- a new CEKF that saturates the filter gain in order to identify feasible joint kinematics and geometrical and inertial parameters of the mechanical model,
- a systematic method for adjusting the measurement and process covariance matrices of the CEKF,
- real-time estimates of the intersegmental moments characterized by an enhanced reliability.

The performance of the proposed CEKF was assessed by determining the accuracy of the estimated GRFM components during the selected motor task. This was made possible by the fact that force-plate recordings were available and, for all practical purposes, could be assumed to be error-free. In addition, the accuracy with which GRFM components are estimated closely depends on the accuracies with which joint kinematics and model parameters are estimated and it is, therefore, a good indicator of the latter accuracies. It should also be emphasised that, due to the large dimension of the CEKF's state vector, it is theoretically possible that accurate GRFM components are provided however accompanied by unrealistic solutions of the state vector. For this reason, the convergence of the kinematic variables estimated by the CEKF towards realistic values was also assessed.

2 Material and methods

2.1 The squat exercise

The experiments involved ten young healthy volunteers (6 males, 4 females, age=33±5 years, mass=71±3 kg, height=1.72 ± 0.04 m). Fourteen reflective markers were located on the right lower and upper limbs and on the torso using a simplified Plug-in-Gait marker-set (Fig. 1). A force-plate (*Bertec Inc*, 1000 Hz) was used to record the GRFM ($\mathbf{FM}=[F_X\ F_Y\ M_Z]^T$), and a stereophotogrammetric system (*9 Mx cameras*, *VICON*, 100 frames/second) simultaneously

recorded the marker trajectories. Volunteers were asked to perform ten consecutive squatting tasks at a self-selected pace and performing the movements in their sagittal plane, parallel to the global frame plane ${}^{G}X{}^{G}Y$, and as symmetrically as possible with respect to it (Fig. 1).

2.2 The mechanical model

A mechanical model of the human locomotor system was created using a planar model composed of seven rigid segments (Fig.1). Segments were connected by seven cylindrical hinges $\boldsymbol{\theta}=[\theta_1\ \theta_2\ \theta_3\ \theta_4\ \theta_5\ \theta_6\ \theta_7]^T$. Toes were assumed to be stationary relative to the ground. The lower limb and shoulder joint centres were determined as in the Plug-in-Gait protocol. The lumbosacral and the abdominal-thoracic joint were determined as the midpoints between the PSI and ASI, and T10 and STR markers, respectively. The elbow joint centre and the metatarsophalangeal joints were made to coincide with the ELB and TOE markers. The head was assumed rigidly attached to the thorax. Segment local frames had the Y axis joining their joint centres and the origin was the proximal joint centre. Their poses were expressed as a function of the segment lengths and joint angles. The positions of the markers in the global reference frame (${}^{G}p_x$, ${}^{G}p_y$) were expressed as a function of their local coordinates (${}^{l}p_x$, ${}^{l}p_y$), segment lengths, and the joint angles. The medio-lateral coordinates resulting from the Plug-in-Gait protocol were disregarded.

FIGURE 1 ABOUT HERE

For each i^{th} segment of the mechanical model, a mass M_i, a moment of inertia around the z-axis ZZ_i, and two components of the first moment of mass (i.e., position of the centre of mass in its local frame multiplied by the corresponding segment mass, MX_i, MY_i) were defined.

2.3 CEKF formulation

The aim of the proposed CEKF is to real-time estimate the state vector composed of the seven (i= 1 … 7) joint angles and derivatives, the segment geometric and inertial parameters, and the fourteen marker local positions (j=1 … 14):

$$\mathbf{x}_{ij} = [\theta_i \; \dot{\theta}_i \; \ddot{\theta}_i \;\; L_i \;\; M_i \; MX_i \; MY_i \; ZZ_i \;\; {}^{l}p_{xj} \;\; {}^{l}p_{yj}]^T, \quad (1)$$

given the artefact-affected marker trajectories in the global frame and the GRFM components as provided by a stereophotogrammetric system and a force-plate, respectively, by minimising the trace of the error covariance matrix **P** (Fig. 2).

FIGURE 2 ABOUT HERE

The next state estimate $\mathbf{x}_{k+1}$ and measurement update $\mathbf{y}_{k+1}$ (where k is the time index varying from k=1... number of samples) are defined as:

$$\mathbf{x}_{k+1} = f(\mathbf{x}_k) + \mathbf{w}_k$$

$$\mathbf{y}_{k+1} = h(\mathbf{x}_k) + \mathbf{v}_k \quad (2)$$

where f is the process model and h is the measurement model. Vectors **w** and **v** represent the process and the measurement noise, assumed to be Gaussian with zero mean and covariance **Q** and **R**, respectively.

The state vector that minimises the least-square difference between the measured and estimated $\boldsymbol{y}$ vector is generated through the two-step prediction-update procedure described in figure 2.

The state update equation assumes that the joint angles and velocities evolve linearly and that joint accelerations and the other parameters are constant. Thus for each segment i and each marker j, the state update vector is

$$\begin{bmatrix} \theta_{ik} \\ \dot{\theta}_{ik} \\ \ddot{\theta}_{ik} \\ L_{ik} \\ M_{ik} \\ MX_{ik} \\ MY_{ik} \\ MZ_{ik} \\ ZZ_{ik} \\ {}^{l}p_{xjk} \\ {}^{l}p_{yjk} \end{bmatrix} = \begin{bmatrix} \begin{bmatrix} 1 & \Delta t & \frac{\Delta t^2}{2} \\ 0 & 1 & \Delta t \\ 0 & 0 & 1 \end{bmatrix} & O_{3x7} \\ O_{7x3} & I_{7x7} \end{bmatrix} \begin{bmatrix} \theta_{ik-1} \\ \dot{\theta}_{ik-1} \\ \ddot{\theta}_{ik-1} \\ L_{ik-1} \\ M_{ik-1} \\ MX_{ik-1} \\ MY_{ik-1} \\ ZZ_{ik-1} \\ {}^{l}p_{xjk-1} \\ {}^{l}p_{yjk-1} \end{bmatrix}, \quad (3)$$

where Δt is the time difference between samples, **0** and **I** are the null and identity matrices, respectively.

The measurement vector at each time step *k* is composed of the measured global marker trajectories, GRFM components, and the subject total mass used as a "soft" constraint.

$$\mathbf{z}_k = [\, {}^{G}p_{xjk} \; {}^{G}p_{yjk} \ldots F_{Xk} \, F_{Yk} \, M_{Zk} \, \textstyle\sum_{i=1}^{7} M_i]^T \quad (4)$$

By adding inequality constraints to the original EKF formulation, the CEKF is created so that it ensures feasible values of the state vector elements. Using a method similar to that proposed by Gupta and Hauser (2007), the following constraints can be implemented:

$$\begin{cases} \mathbf{A}_{KF}\hat{\mathbf{x}}_{k|k} = \mathbf{b} \\ \mathbf{C}_{KF}\hat{\mathbf{x}}_{k|k} \leq \mathbf{d} \end{cases} \quad (5)$$

where **b** and **d** are equality and inequality constraint vectors, respectively.

At each time step, the Kalman gain and state update were computed and the element of the updated state vector were checked to be within their constraint limits. Then, if one element of the state vector was not within its limits, the vector **b**, initially set to zero, was updated with the corresponding limit value, the Kalman gain and the state vector were then re-computed as

$$\mathbf{K}_k^R = \mathbf{K}_k - \mathbf{A}_{KF}^T(\mathbf{A}_{KF}\mathbf{A}_{KF}^T)^{-1}\left(\mathbf{A}_{KF}\hat{\mathbf{x}}_{k|k} - \mathbf{b}\right)(\mathbf{v}_k{}^T\mathbf{S}_k{}^{-1}\mathbf{v}_k)^{-1}\mathbf{v}_k{}^T\mathbf{S}_k{}^{-1} \quad (6)$$

$$\hat{\mathbf{x}}_{k|k}^R = \hat{\mathbf{x}}_{k|k} + \mathbf{K}_k^R\mathbf{v}_k \quad (7)$$

Constraints on the segment lengths and BSIP values were set using anthropometric tables (Dumas et al., 2007) and a threshold of +/-20 %, the maximal and minimal local markers positions ($^{l}\boldsymbol{L}$, $^{l}\mathbf{U}$) were constrained to lie within the segment maximal length and width:

$$\begin{cases} \theta_{li} < \theta_i < \theta_{ui} \\ L_{ATi} - 0.2L_{ATi} \leq L_i \leq L_{ATi} + 0.2L_{ATi} \\ {}^{l}L_{xj} \leq {}^{l}p_{xj} \leq {}^{l}U_{xj} \\ {}^{l}L_{yj} \leq {}^{l}p_{yj} \leq {}^{l}U_{yj} \\ M_{ATi} - 0.2M_{ATi} \leq M_i \leq M_{ATi} + 0.2M_{ATi} \\ MX_{ATi} - 0.2MX_{ATi} \leq MX_i \leq MX_{ATi} + 0.2MX_{ATi} \\ MY_{ATi} - 0.2MY_{ATi} \leq MY_i \leq MY_{ATi} + 0.2MY_{ATi} \\ ZZ_{ATi} - 0.2ZZ_{ATi} \leq ZZ_i \leq ZZ_{ATi} + 0.2ZZ_{ATi} \end{cases} \quad (8)$$

where the subscript AT denotes parameters estimated using an anthropometric table, θ_{li} and θ_{ui} are lower and upper joint angle boundary values.

2.4 CEKF parameter adjustment

The parameters governing the CEKF behaviour are embodied in the process covariance matrix **Q,** the measurement covariance matrix **R**, and the initial values of the state vector $\mathbf{x}_1$ and state covariance matrix **P**. Parameter adjustment of the CEKF is of crucial importance since the noise parameters influence the filter stability and its convergence rate. The measurement covariance matrix **R** for the stereophotogrammetric system is usually set using the system's noise. However, this is not appropriate as it fails to consider the additional noise introduced by the STA. Accordingly, the elements of **R** were given values describing the STA taken from the literature (Table 1). For the force-plate data the measurement noise provided by the manufacturer was used.

Since the segment lengths, local positions of the markers, and BSIP are independent they should converge to a constant value. Conveniently, the error covariance matrix **P** will converge to zero for constant terms if elements of **Q** are set to zero (Southall et al., 1998). Process covariance values related to the evolution of the joint angles and derivatives ($\boldsymbol{Q_{\theta}}, \boldsymbol{Q_{\dot{\theta}}}, \boldsymbol{Q_{\ddot{\theta}}}$) should be much larger to reflect the errors due to the constant acceleration assumption (eq.3). Therefore the process noise given by De Groote et al. (2008) can be used to determine **Q**:

$$\boldsymbol{Q}_j = \sigma^2 \mathbf{G}^T \mathbf{G} \text{ with } \mathbf{G} = \begin{bmatrix} \frac{\Delta t^3}{3} & \frac{\Delta t^2}{2} & \Delta t \end{bmatrix} \quad (9)$$

The value σ^2 can be set up *a priori* if the maximal frequency content of the signal, ω_{max}, the power spectral amplitude A, and the sampling frequency are known (Cerveri et al., 2003):

$$\sigma^2 = \frac{(A{\omega_{max}}^4 e^{\omega_{max}\Delta t})^2}{3\Delta t} \quad (10)$$

During a squat, ω_{max} =1 Hz can be assumed, and the maximal power spectral amplitude can be approximated from the fast Fourier transform of a representative joint angle curve of the knee calculated with the marker method. Finally, σ^2 was set to 1.10^3 for all the joints. The proposed CEKF receives as input both kinematic and kinetic data, thus it is crucial to normalize the data: the rows of **R,** that correspond to marker data were scaled with a parameter α and the ones corresponding to the measured GRFM with a parameter β. The best threshold value of the *RMSD* between estimated and measured marker trajectories and components of the GRFM was determined iteratively. The coefficients were varied from 0 to 5.10^{-3} using a Monte-Carlo simulation with 10^3 different combinations.

For all the analyses, CEKF initial state vector values were set using the marker positions at the first sample of time to define an initial segment orientation and length. From the pose of the local frames, a first guess on the local marker positions was extrapolated. Finally, initial joint velocities and accelerations were assumed to be null at the first time step, and anthropometric table values (Dumas et al., 2007) were used to set the initial BSIP values.

The initial error covariance matrix can be adjusted to improve EKF convergence rate. A low value of **P** will indicate that the corresponding state variable value can be trusted. Thus, the initial values of the state covariance matrix **P** were set using an approximate percentage of the uncertainties on the estimate of each parameter. For the joint kinematics variables, segment lengths and local marker positions, the initial state covariance matrix was set assuming an error of 20% of their initial value. The rows of the initial state covariance matrix **P** corresponding to each BSIP were set according to the findings of Riemer et al. (2008), who have compared the BSIP of several anthropomorphic tables.

2.5 Analysis

Using the CEKF optimized joint angular positions, velocities, and accelerations, segment lengths, and BSIP and a top-down recursive Newton-Euler method, the GRFM ($\mathbf{FM_f} = [F_{fX}\ F_{fY}\ M_{fZ}]^T$) and the lower limb and lumbosacral joint intersegmental moments ($\mathbf{\Gamma_f}$) were estimated.

For comparison purposes the above-mentioned variables were also estimated using a classical method. The joint angles $\boldsymbol{\theta_c}$, were calculated using the pose of the segment local frames determined using the raw stereophotogrammetric data. These angles were differentiated and filtered (Butterworth-5th order, 10Hz) using a first order centred method. BSIPs were estimated using an anthropometric table (Dumas et al., 2007). Using these variables and parameters and a classical top-down approach, the GRFM ($\mathbf{FM}_c$) were estimated. The lower limb and lumbosacral joint intersegmental moments ($\mathbf{\Gamma_c}$) were estimated using a bottom-up approach and the measured GRFM.

The root mean square (*RMSD*) and the normalised root mean square differences (*NRMSD*), and the correlation coefficient (*r*) between the raw global marker positions and those estimated using the kinematic variables estimated by the CEKF, were calculated in order to determine the ability of the algorithm to converge to a realistic solution.

The ability of the proposed method to attenuate the effects of experimental errors and artefacts, and the model parameter estimation errors was assessed by analysing the *RMSD* and the *NRMSD* between the CEKF estimated ($\mathbf{FM}_f$) and the measured values of the GRFM (**FM**); the latter were regarded as the true values. The *RMSDs* and the *NRMSDs* between the GRFM estimates ($\mathbf{FM}_c$) obtained using the classical method and the corresponding measured values (**FM**), and between the intersegmental moments at the lower limb and lumbosacral joints ($\mathbf{\Gamma_f}$) based on CEKF output and those obtained using the classical method ($\mathbf{\Gamma_c}$), were also computed.

3 Results

3.1 CEKF parameter adjustment

Figure 3 presents the sensitivity analysis of the weighting between the kinematic and kinetic measured quantities. Out of 10^3 weight combinations, 159 were not displayed since they led to

filter instabilities. An L-shaped curve can be observed in figure 3a that describes the *RMSD* between the measured and estimated marker trajectories and components of the GRFM for all α and β combinations. The inflection point of the L-curve shows the existence of an optimal trade-off between the tracking of kinematic and kinetic data. When the error in both quantities increases a linear tendency is observable. This can be explained by the fact that the kinematic and dynamic models are intrinsically linked through the joint angles and segment lengths. Figures 3b and 3c show the evolution of each of the *RMSD* depending on α and β. The sum of the *RMSD* between estimated and measured GRFM is unitless. In order to find a less subject specific tuning of the α and β weights the following normalization is proposed:

$$\alpha = (N_M H_B)^2$$
$$\beta = (W_B)^2 \quad (11)$$

where N_M, H_B, and H_B are the number of markers, and body height [m] and mass [kg], respectively. For the subject used for the sensitivity analysis, α and β are set at 635 and 4900, respectively, as indicated in figure 3 by the black cross. Even though these values do not match the inflection point of the L-curve exactly, the *RMSD* values given by this choice were very low (*RMSD* GRFM = 1.8; *RMSD* markers = 2.7 mm). The differences between the marker tracking *RMSD* calculated at the black cross point and at the exact curve inflexion point (1.9 mm) are within the accuracy of the stereophotogrammetric system and can be neglected. Consequently, for the subsequent analyses α and β were adjusted using the BH, and BW of each subject.

3.2 Assessment

Table 2 summarizes the differences between the CEKF estimated and measured global coordinates of the markers. It is shown that CEKF is able to track the marker trajectories with an average *RMSD* of 3±2mm, with the maximal *NRMSD* value observed for the heel and shoulder markers.

The discrepancy between the components of the GRFM estimated using the proposed method

($\mathbf{FM_f}$) and the classical method ($\mathbf{FM_c}$) and the corresponding measured values is illustrated in figure 4 and Table 3. An average *RMSD* between $\mathbf{FM_f}$ and **FM** of 3.4 N, 8.6 N and 9.5 Nm, for F_X, F_Y, and M_Z, respectively, was found. These values were at least 2.5 times smaller than the $\mathbf{FM_c}$ components, obtained using the classical method. Differences were larger for F_X and M_Z. The correlation coefficients were on average higher than 0.92 for all variables with the lowest value of 0.77 for F_X. In figure 4 it can be observed that after a short period of time (approximately 2 s) the CEKF successfully converged toward the measured values.

Figure 4 and Table 3 also report the results of the comparison between the lower limb and lumbosacral intersegmental moments estimated using the CEKF outputs and the top-down method ($\mathbf{\Gamma_f}$) and the bottom-up classical method ($\mathbf{\Gamma_c}$).

Figure 5 depicts the joint angles as estimated by the CEKF and as calculated using raw stereophotogrammetric data (classical method). The corresponding *RMSD*, *NRMSD* and *r* between CM and CEKF estimates were for θ_1: 0.01 rad, 10 %, and 0.99; for θ_2: 0.05, 2%, 0.97; for θ_3: 0.19, 28%, and 0.99; for θ_4: 0.08, 9 %, and 0.98; for θ_5: 0.33, 56%, and 0.32; for θ_6: 0.07, 21%, and 0.26; and for θ_7: 0.05, 21%, and 0.93.

Figures 6 and 7 show how the model parameters vary during the first four squats of the series of ten for a randomly chosen subject. It can be seen that the BSIP are only slightly modified within the CEKF procedure. On the other hand, some lower limb segment lengths are modified substantially by cause of the inaccuracy of the initial values. Nevertheless all parameters converge towards a constant value after approximately 5 s. This is expected since the corresponding elements of the process covariance matrix **Q** were set to zero (Table 1).

4 Discussion

The estimation of joint kinematics and intersegmental moments using conventional motion analysis techniques is prone to experimental and modelling errors, typically associated with the STAs and the estimated BSIP. In the literature, both multi-body optimization and EKF have been

proposed to compensate for the STA. In the proposed CEKF, all the state variables can be modified together to optimally track the STA-affected marker trajectories. Therefore, the *RMSD* can be further minimised because the segment lengths and the local positions of the markers were not strictly constant. Nevertheless, by setting to 0 the corresponding **Q** lines of the segment lengths, of the local marker positions, and of the BSIP, these parameters globally converge toward constant values. It was expected that, thanks to the model mechanical constraints and the introduction of kinetic input data, the STA would have had a reduced influence. However, since no model of the STA is embedded in the proposed CEKF, STA is not completely compensated for. This is reflected in the 3±2 mm *RMSD* on the marker trajectories as well as in the oscillations of the segment lengths. The total lower-limb length varies by 3 cm and after a few seconds converges toward a constant value. This can be due to the inaccuracy of the initial values of the geometrical parameters. Nevertheless, this variation is lower than the variation of the segment lengths that might be caused by the STA and by the incorrect estimate of the hip joint centre. One possible solution to further limit the impact of the STA on the identification of the segment lengths and BSIP could be to allow for the alteration of the local positions of the markers by setting the corresponding **Q** values not to be null.

Further investigations should be carried out to compare our method with more advanced multi-body optimization methods (Andersen et al., 2010a, Reinbolt et al., 2005). However, there is a serious gap in the literature regarding the tuning of the weights introduced to reflect the error distribution among the markers. For multi-body optimization methods that do not identify the geometrical parameters, the reported *RMS* errors affecting knee kinematics range between 1 and 23 degrees (Andersen et al. 2010b, Li et al. 2012, Gasparutto et al., 2015, Clément et al., 2015, Richard et al., 2016, Clément et al., 2017). The maximal errors were obtained for subjects performing squatting activities as in the present study.

Our method allows also to simultaneously identify the BSIPs that have a non-negligible influence on the accuracy of inverse dynamics outcome. The BSIP values estimated in this study do not strongly evolve from their initial values, set from anthropometric tables. This may be due to the fact that our subjects fit the population used to produce that table or to the fact that the solution of the CEKF procedure is not unique. In addition, the oversimplified model might degrade the estimate of the BSIP. However, for small relative motions it has been shown that some of the

BSIPs, and typically head and trunk BSIPs during squat, regroup themselves in the so-called base-parameters (Bonnet et al., 2015). In the case of the analysed squat exercise, the motion may not have excited all of the BSIP. The intersegmental moments were modified by about 20Nm, i.e., up to 60%, at the hip joint. This difference is comparable to the results of the sensitivity analyses reported in the literature that altered both BSIPs and segment lengths (Riemer et al. 2008).

In conclusion, from the results presented herein it may be inferred that the proposed CEKF allows for a significant improvement of the accuracy with which kinematic variables and relevant time derivatives, model parameters and, therefore, intersegmental moments are estimated. This has been shown with reference to a sagittal symmetric exercise and using a 2D model. However, the CEKF is, in principle, applicable to a 3D model as well although this would entail considerably more parameters in the procedure and may exhibit a redundancy problem.

Conflict of interest statement

No party having a direct interest in the results of the research supporting this article has or will confer a benefit on the author(s) or on any organization with which the author(s) is/are associated.

ACKNOWLEDGMENTS

This study was supported by the Japan Society for Promotion of Science (No PE13559) and by the JSPS-MAEDI bilateral program 2015-2016.

References

Andersen M.S., Damsgaard M., MacWilliams B., Rasmussen J., 2010a. A computationally efficient optimisation-based method for parameter identification of kinematically determinate and over-determinate biomechanical systems. Comput. Method. Biomec. 13, 171-183.

Andersen M.S., Benoit D.L., Damsgaard M., Ramsey D.K., Rasmussen J., 2010b. Do

kinematic models reduce the effects of soft tissue artefacts in skin marker-based motion analysis? An in vivo study of knee kinematics. J. Biomech. 43, 268–273.

Ayusawa K., Venture G., Nakamura Y., 2013. Identifiability and identification of inertial parameters using the underactuated base-link dynamics for legged multibody systems**.** Int. J. Robot. Res. 33, 446-468.

Bonnet V., Venture. G., 2015. Fast determination of the planar body segment inertial parameters using affordable sensors. IEEE Trans. Neural Syst. Rehabil. Eng. 23, 628-635.

Cahouet V., Martin L., Amarantini D., 2002. Static optimal estimation of joint accelerations for inverse dynamics problem solution. J. Biomech. 35, 1507-1513.

Cerveri P., Pedotti A., Ferrigno G., 2005. Kinematical models to reduce the effect of skin artifacts on marker based human motion estimation. J. Biomech. 38, 2228–2236.

Cerveri P., Pedotti A., Ferrigno G., 2003. Robust recovery of human motion from video using Kalman filters and virtual humans. Hum. Mov. Sci. 22, 377-404.

Clément J., Dumas R., Hagemesiter N., de Guise J.A., 2015. Soft tissue artifact compensation in knee kinematics by multi-body optimization: Performance of subject-specific knee joint models. J. Biomech. 48, 3796-3802.

Clément J., Dumas R., Hagemeister N., de Guise J.A., 2017. Can generic knee joint models improve the measurement of osteoarthritic knee kinematics during squatting activity? Comput. Methods Biomech. Biomed Engin. 20, 94-103.

De Groote F., Laet T.D., Jonkers I., Schutter J.D., 2008. Kalman smoothing improves the estimation of joint kinematics and kinetics in marker-based human gait analysis. J. Biomech. 41, 3390-3398.

Dumas R., Chèze L., Verriest J., 2007. Adjustments to McConville et al. and Young et al. body segment inertial parameters. J. Biomech. 40, 543–553.

Fohanno V., Begon M., Lacouture P., Colloud F., 2014. Estimating joint kinematics of a

whole body chain model with a closed-loop constraints. Multibody Syst. Dynamics 31, 433-449.

Gasparutto X., Sancisi N., Jacquelin E., Parenti-Castelli V., Dumas R., 2015. Validation of a multi-body optimization with knee kinematics models including ligament constraints. J. Biomech. 48, 1141-1146.

Gupta N., Hauser R., 2007. Kalman filtering with equality and inequality state constraints. Arxiv, http://arxiv.org/abs/0709. 2791.

Hara R., Sangeux M., Baker R., Mc Ginley J., 2014. Quantification of pelvic soft tissue artifact in multiple static positions. Gait Posture 39, 712-717.

Kuo A.D., 1998. A least-squares estimation approach to improving the precision of inverse dynamics computations. J. Biomech. Eng. 120, 148-159.

Lamberto G., Martelli S., Cappozzo A., Mazzà C., 2016. To what extent is joint and muscle mechanics predicted by musculoskeletal models sensitive to soft tissue artefacts? J Biomech. doi: 10.1016/j.jbiomech.2016.07.042.

Li K., Zheng L., Tashman S., Zhang X., 2012. The inaccuracy of surface-measured model-derived tibiofemoral kinematics. J. Biomech. 45, 2719-2723.

Lu, T.W., O'Connor, J.J., 1999. Bone position estimation from skin marker co-ordinates using global optimisation with joint constraints. J. Biomech. 32, 129–134.

Peters A., Galna B., Sangeux M., Morris M., Baker R., 2010. Quantification of soft tissue artifact in lower limb human motion analysis: A systematic review. Gait Posture 31, 1-8.

Reinbolt J.A., Schutte J.F., Fregly B.J., Koh B., Haftka R.T., George A.D., Mitchell, K.H., 2005. Determination of patient-specific multi-joint kinematic models through two-level optimization. J. Biomech. 38, 621-626.

Richard V., Lamberto G., Lu T.W., Cappozzo A., Dumas R., 2016. Knees kinematics estimation using multi-body optimisation embedding a knee joint stiffness matrix: a

feasibility study. Plos One, DOI:10.1371/journal.pone.01570.

Riemer R., Hsiao-Wecksler E.T., Zhang X., 2008. Uncertainties in inverse dynamics solutions: a comprehensive analysis and an application to gait. Gait Posture 27, 578-588.

Robert T., Chèze L., Dumas R., Verriest J.P., 2007. Validation of net joint loads calculated by inverse dynamics in case of complex movements: Application to balance recovery movements. J. Biomech. 40, 2450-2456.

Simon D., 2010. Kalman filtering with state constraints: a survey of linear and nonlinear algorithms. IET Control Theory Applications 4, 1303-1318.

Southall B., Buxton B.F., Marchant J.A., 1998. Controllability and observability: Tools for Kalman filter design. In Proc. British Machine Conf., 1-10.

Stagni R., Leardini A., Cappozzo A., Benedetti M.G., Cappello A., 2000. Effects of hip joint centre mislocation on gait analysis results. J. Biomech. 33, 1479-1487.

Zemp R., Gülay T., Elsig J.P., Naxera J., Taylor W.R., Lorenzetti S., 2014. Soft Tissue Artefacts of the Human Back: Comparison of the Sagittal Curvature of the Spine Measured Using Skin Markers and an Open Upright MRI. Plos One 9, DOI:10.1371/journal.pone.0095426.

FIGURE LEGENDS

Fig. 1. Seven-degree-of-freedom model of the human body used to analyse a squat exercise. Joint angles $\boldsymbol{\theta}$ and segment lengths $\boldsymbol{L}$ are represented in (a) and (b), respectively. Figure c shows the segment definitions and the marker set.

Fig. 2. Overview of the proposed constrained extended Kalman filter (CEKF). $\hat{\mathbf{x}}_{k|k}$, $\mathbf{P}_{k|k}$ and $\mathbf{K}_k$ are the predicted mean and covariance of the state vector and the CEKF gain matrix, respectively. **H** and **F** are the Jacobian matrices of *f* and *h* calculated symbolically relative to the state vector.

Fig. 3. Results of the sensitivity analysis performed to determine the weights trade-off between the kinematic and kinetic measured data. The black cross indicates the weight values chosen accounting for subject body mass and height. (a) Each grey dot indicates an α and β combination with corresponding *RMSD* between measured and estimated marker trajectories and GRFM. (b and c) Evolution of the *RMSD* between measured and estimated marker trajectories and GRFM as a function of α and β.

Fig. 4. Results for a randomly chosen participant showing the GRFM components estimated using the proposed CEKF ($\mathbf{FM_f}$), estimated using the classical top-down method (CM) ($\mathbf{FM_c}$), and measured using a force-plate (**FM**). The lower limb and lumbosacral intersegmental moments (ankle: Γ_2; knee: Γ_3; hip: Γ_4; lumbosacral joint: Γ_5) estimated using the CEKF ($\boldsymbol{\Gamma_f}$) and the bottom-up classical method ($\boldsymbol{\Gamma_c}$) are also illustrated. The first four squats of the series of ten are shown.

Fig. 5. Results relative to a randomly chosen volunteer showing the joint angles (Fig.1) estimated using the proposed filter (CEKF) and estimated using the classical method (CM). The first four squats of the series of ten are shown.

Fig. 6. Results for a randomly chosen participant showing the time evolution of the segment mass and length estimates. The first four squats of the series of ten are shown.

Fig. 7. Results for a randomly chosen participant showing the time evolution of the segment first and second moment of inertia estimates. The first four squats of the series of ten are shown.

Table 1 Gain values of the measurement (**R**) and process (**Q**) covariance matrices used to adjust the CEKF behaviour. Expected soft tissue artefact (STA) influence for each marker and the force-plate measurement noise used to fill the measurement matrix are taken from the quoted publications. The elements of the process covariance matrix relative to the joint kinematics are determined using equation 9 and set to zero if relative to the constant geometrical and inertial parameters.

	Value	Description	Data Source
R_{TOE}	1.10^{-3}	Toe marker	Peters et al., 2010
R_{HEE}	$2.7.10^{-3}$	Heel marker	Peters et al., 2010
R_{ANK}	10.10^{-3}	Ankle marker	Peters et al., 2010
R_{SHA}	15.10^{-3}	Shank marker	Peters et al., 2010
R_{KNE}	30.10^{-3}	Knee marker	Peters et al., 2010
R_{THI}	11.10^{-3}	Thigh marker	Peters et al., 2010
R_{PSI}	1.10^{-3}	Posterior pelvis marker	Hara et al., 2014
R_{ASI}	17.10^{-3}	Anterior pelvis marker	Hara et al., 2014
R_{T10}	$10.7.10^{-3}$	T10 marker	Zemp et al., 2014
R_{STR}	15.10^{-3}	Sternum marker	Zemp et al., 2014
R_{C7}	15.10^{-3}	C7 marker	Zemp et al., 2014
R_{CLA}	9.10^{-3}	Clavicle marker	Zemp et al., 2014
R_{SHO}	27.10^{-3}	Acromion marker	Zemp et al., 2014
R_{ELB}	10.10^{-3}	Elbow marker	empirical
R_{FX}	0.1	Horizontal GRF	manufacturer
R_{FY}	0.1	Vertical GRF	manufacturer
R_{MZ}	0.1	Ground resultant moment	manufacturer
R_{Mtot}	1.10^{-4}	Mass soft constraint	empirical
$Q_{\theta,}\ Q_{\dot{\theta},}\ Q_{\ddot{\theta}}$	1.10^{3}	Joint, velocity and acceleration	Cerveri et al., 2003
Q_L	0	Lengths and inertial parameters	Southall et al., 1998
Q_p	0	Local marker coordinates	Southall et al., 1998

Table 2 Results of the comparison between the measured and CEKF estimated global X and Y marker coordinates. Results have been reported as mean±SD over all the analysed squat trials and volunteers.

	RMSD [mm]		*NRMSD* [%]		*r*	
	X	Y	X	Y	X	Y
TOE	0.0±0.0	0.0±0.0	0.0±0.0	0.0±0.0	1.0±0.0	1.0±0.0
HEE	5.3±2.1	3.7±1.4	46.0±28.1	4.7±2.3	0.83±0.12	0.93±0.11
ANK	0.6±0.2	0.7±0.6	0.4±0.1	2.0±1.6	0.92±0.24	0.76±0.26
SHA	3.6±1.9	2.5±1.4	2.6±1.5	0.9±0.5	0.94±0.19	0.93±0.21
KNE	5.0±2.3	2.5±1.2	4.7±2.3	0.5±0.2	0.95±0.18	0.95±0.16
THI	0.9±0.6	1.9±1.8	6.2±4.9	0.5±0.2	0.94±0.19	0.98±0.01
PSI	4.1±2.9	4.0±1.2	1.8±1.3	0.4±0.1	0.96±0.05	0.95±0.18
ASI	4.7±3.3	4.6±2.3	10.1±7.5	0.5±0.2	0.97±0.04	0.99±0.02
T10	3.9±3.2	2.6±1.4	1.9±1.7	0.2±0.1	0.92±0.09	0.95±0.17
STR	5.8±3.5	2.3±0.6	12.7±8.2	0.2±0.0	0.88±0.11	0.96±0.11
C7	5.4±3.2	2.2±1.2	3.7±3.3	0.2±0.0	0.94±0.13	0.92±0.31
CLA	5.5±4.3	1.9±0.6	17.0±0.0	0.1±0.0	0.93±0.11	0.97±0.09
SHO	5.1±3.9	2.5±1.1	17.2±8.8	0.1±0.0	0.93±0.12	0.98±0.03
ELB	5.2±3.9	4.2±2.1	6.7±4.7	0.2±0.0	0.87±0.18	0.87±0.18

Table 3 Root mean square (*RMSD*) and normalized root mean square difference (*NRMSD*) between ground reaction force and moment components (F_X, F_Y, M_Z) estimated using the CEKF and a classical top-down recursive Newton-Euler method (CM) and the corresponding measured values. The difference between the lower limb and lumbosacral intersegmental moments estimated using the CEKF ($\boldsymbol{\Gamma_f}$) and the bottom-up classical method ($\boldsymbol{\Gamma_c}$) is also illustrated. Results have been reported as mean±SD over all the analysed squat trials and volunteers.

		RMSD	*NRMSD* [%]	*r*
F_X	CEKF	3.4±4.4 [N]	33±8	0.77±0.13
	CM	10.5±6.4 [N]	44±27	0.12±0.09
F_Y	CEKF	8.6±9.31 [N]	1.19±2.98	0.99±0.01
	CM	21.6±20 [N]	3.0±2.4	0.96±0.02
M_Z	CEKF	9.5±12.4 [Nm]	12.6±10.7	0.85±0.02
	CM	29.2±25.3 [Nm]	26.7±15.0	0.62±0.19
Γ_2(Ankle)		17.3±11.9 [Nm]	33.9±17.2	0.74±0.14
Γ_3(Knee)		24.5±1.47 [Nm]	39.0±19.7	0.94±0.07
Γ_4(Hip)		21.4±11.9 [Nm]	59.6±28.5	0.77±0.24
Γ_5(Lumbosacral)		11.0±7.6 [Nm]	56.3±37.6	0.78±0.23

Figure 1

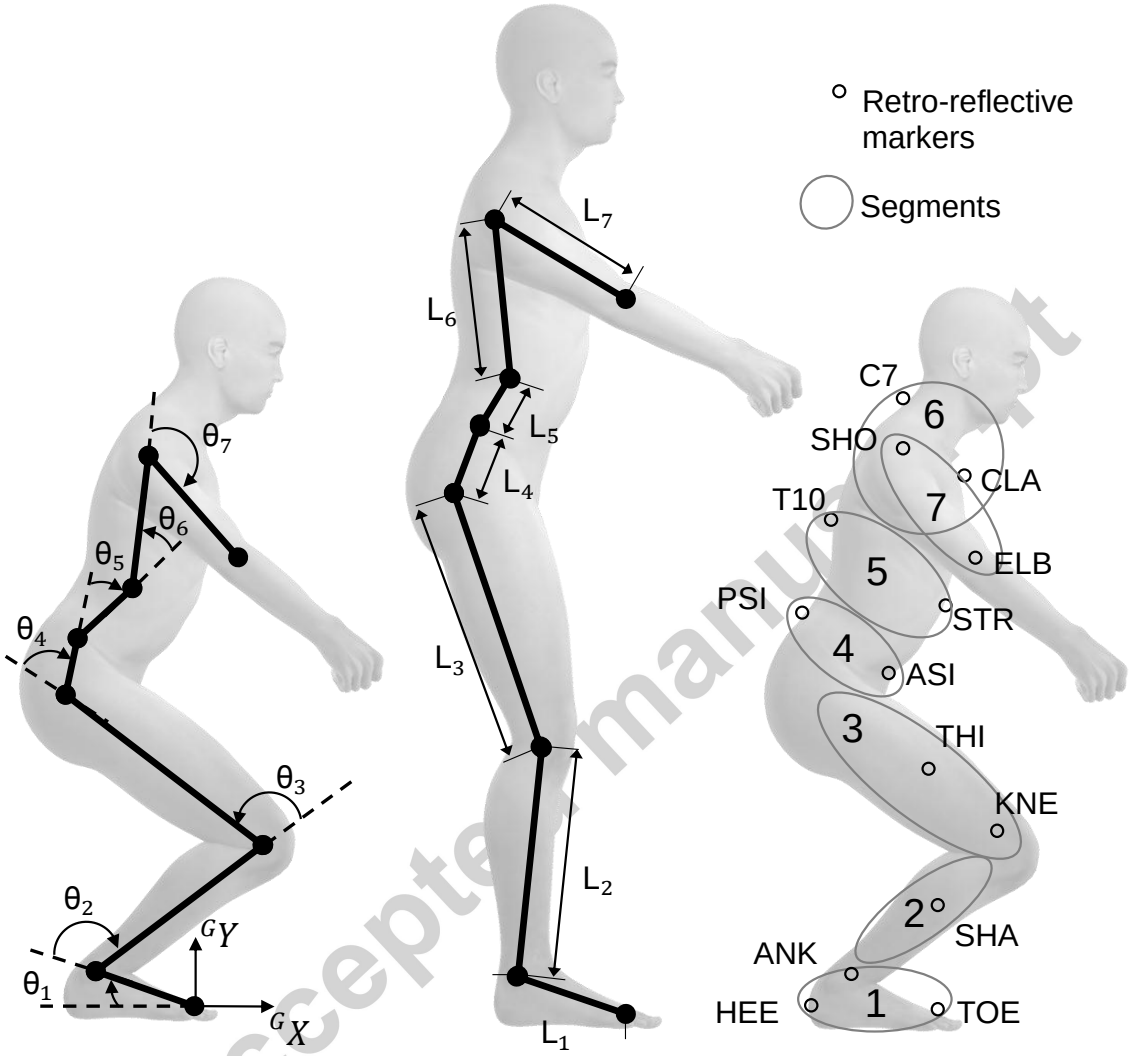

(a) Crouch position (b) Initial/final position (c) Segments definition

Figure 2

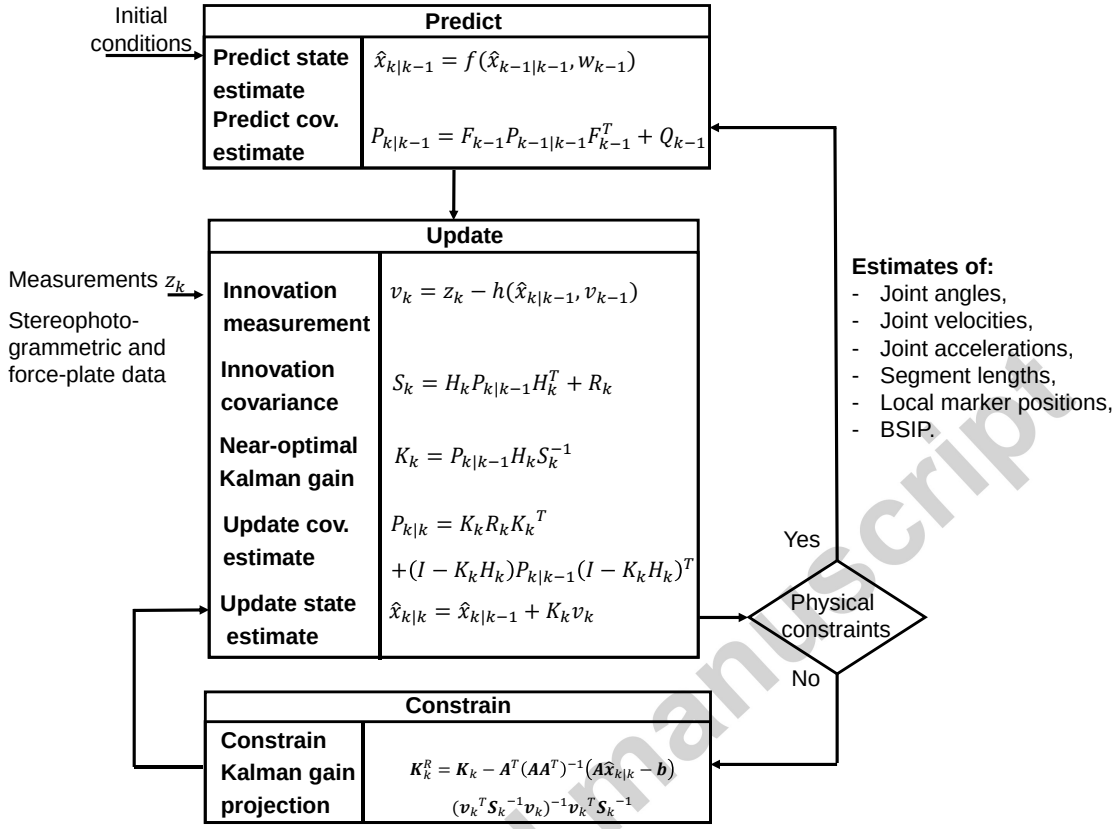

Figure 3

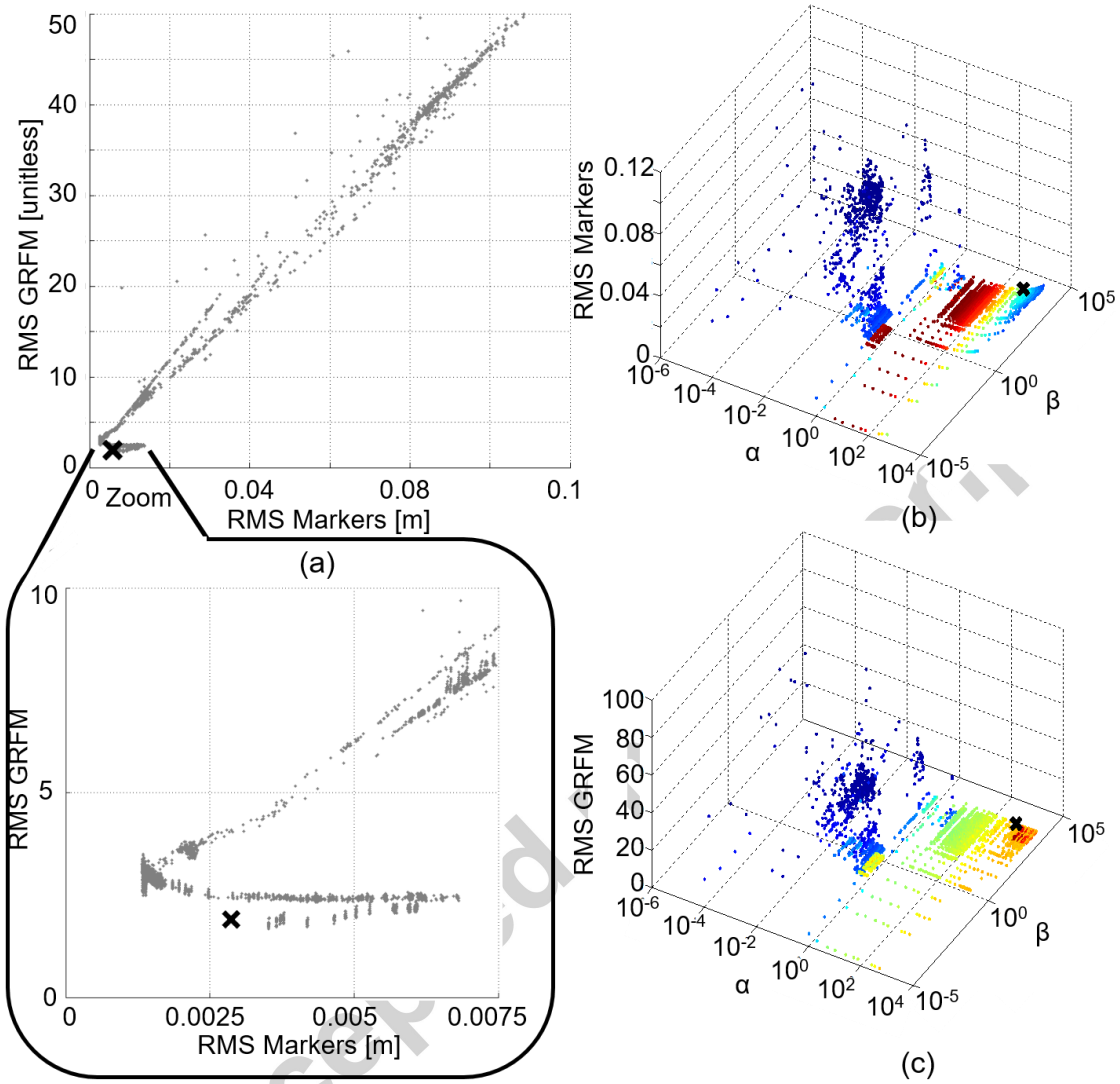

Figure 4

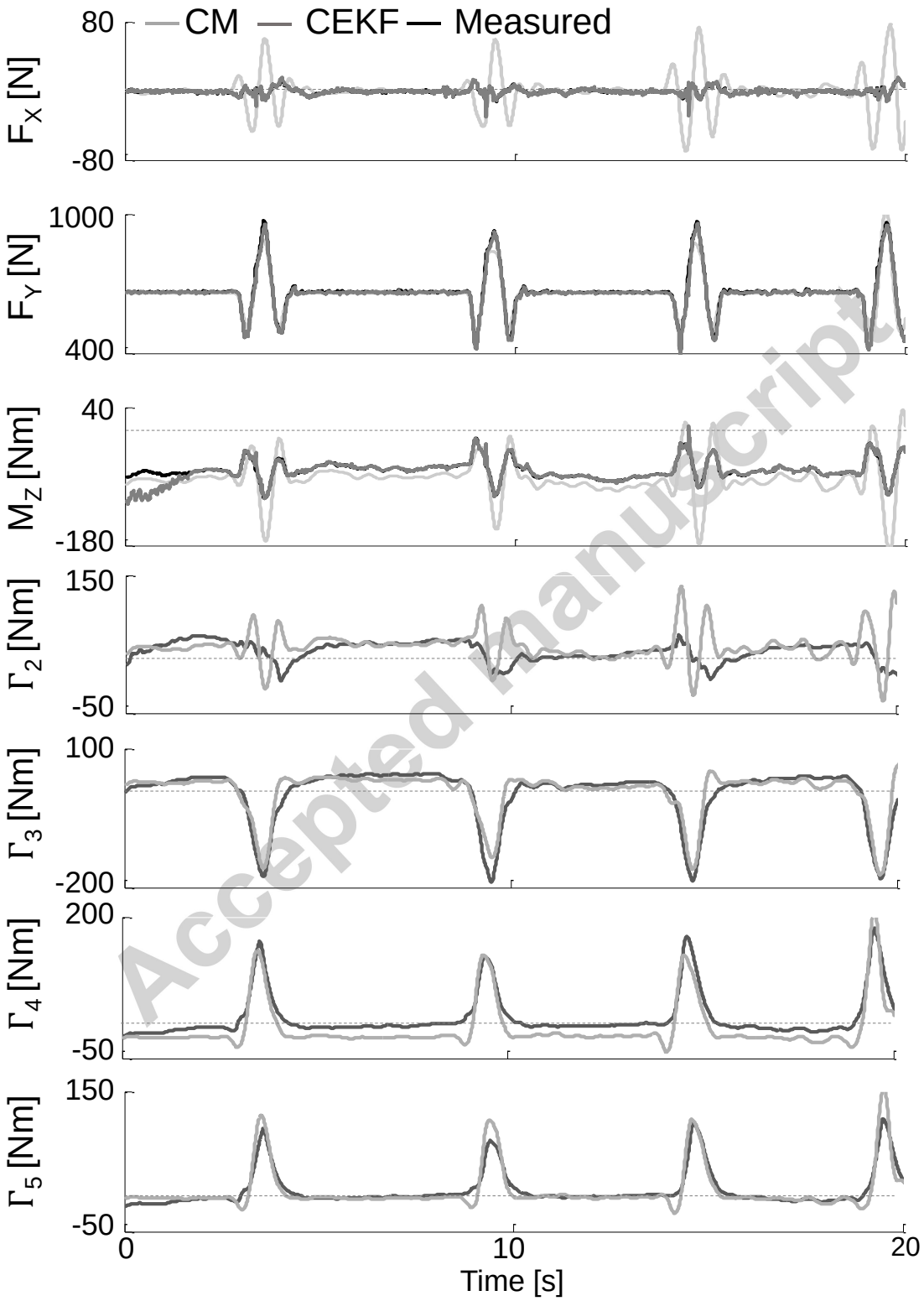

Figure 5

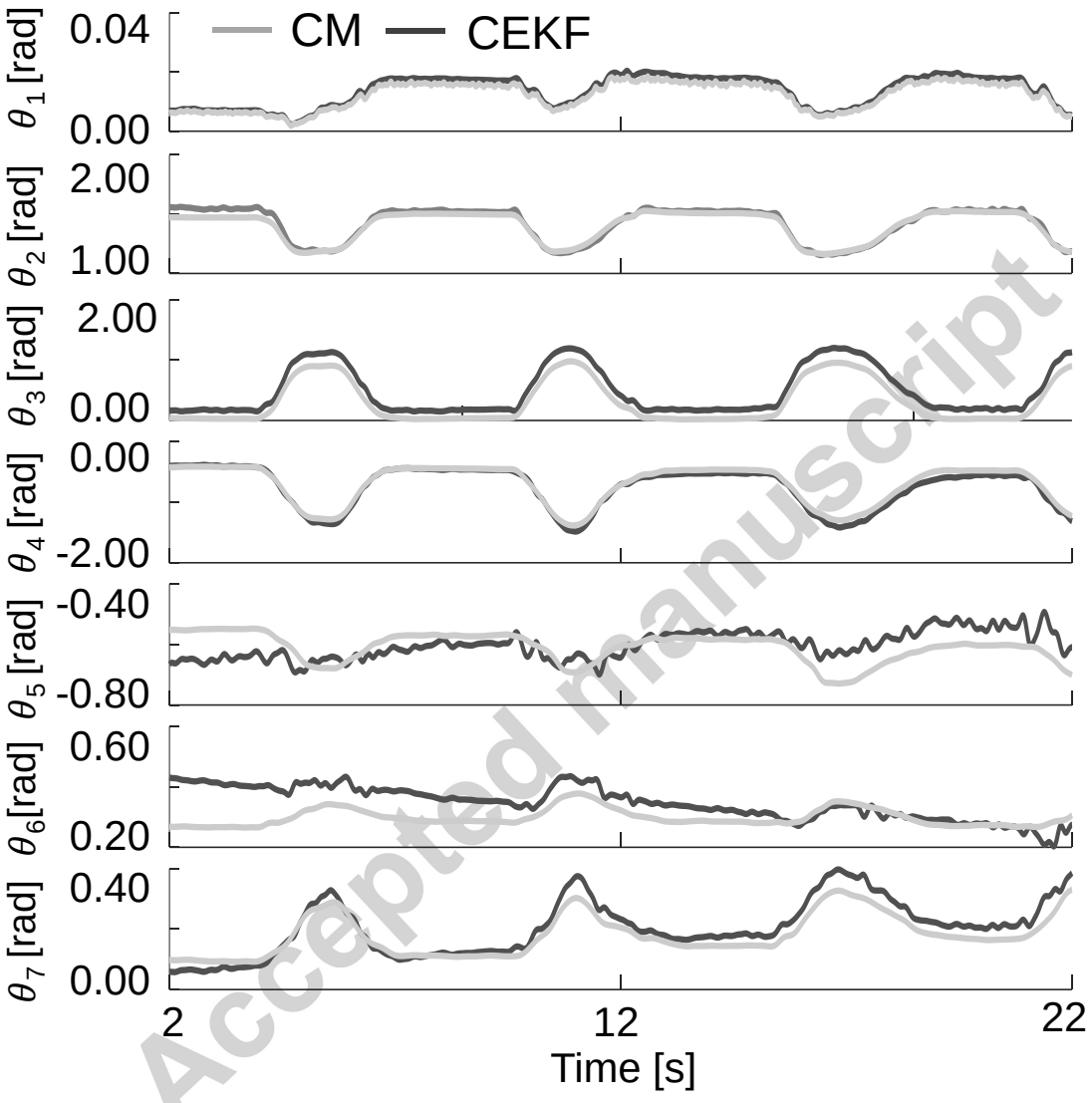

Figure 6

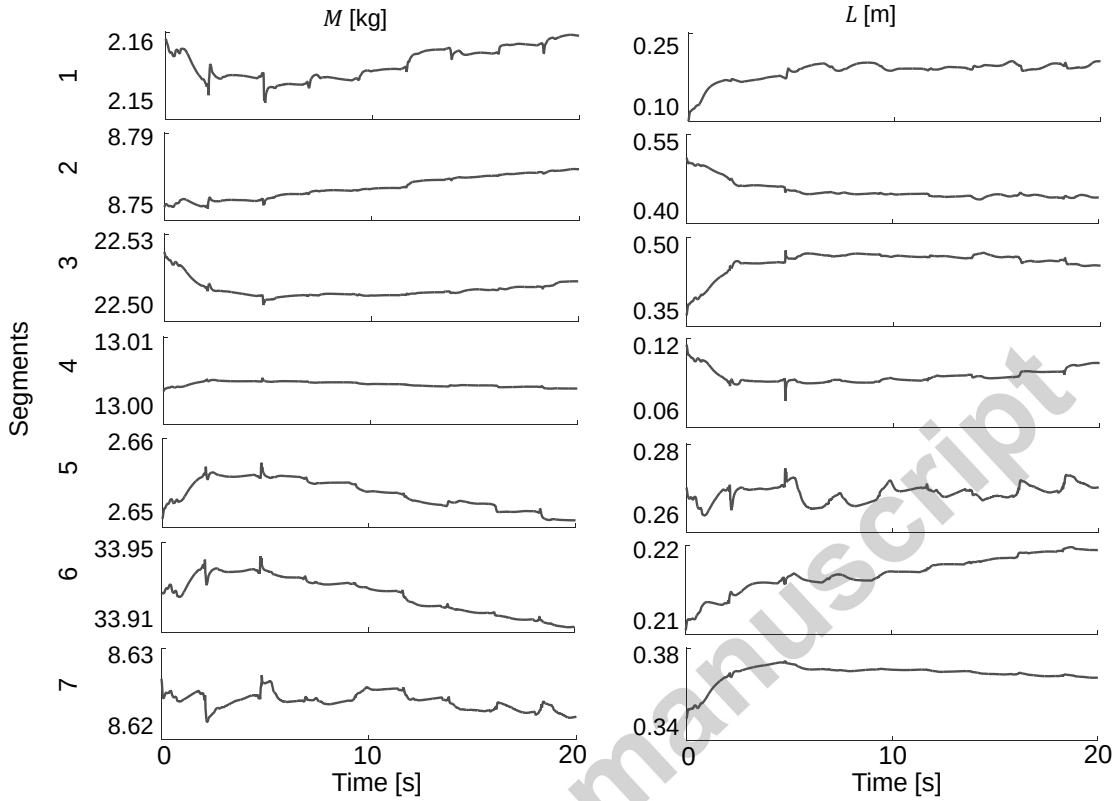

Figure 7